01 Apr 2008

Dual-Function Neuron-Based External Controller for a Static Var Compensator

Ganesh K. Venayagamoorthy
Missouri University of Science and Technology

Sandhya R. Jetti

Dual-Function Neuron-Based External Controller for a Static Var Compensator

Ganesh Kumar Venayagamoorthy, *Senior Member, IEEE*, and Sandhya Rani Jetti, *Student Member, IEEE*

***Abstract*—The use of wide-area measurements for power system stabilization has recently been given a lot of attention by researchers and the power industry to avoid cascading failures and blackouts, such as the one in North America in August 2003. This paper presents the design of a nonlinear external damping controller based on wide-area measurements as inputs to a single dual-function neuron (DFN)-based controller. This DFN controller is specifically designed to enhance the damping characteristics of a power system over a wide range of operating conditions using an existing static var compensator (SVC) installation. The major advantage of the DFN controller is that it is simple in structure with less development time and hardware requirements for real-time implementation. The DFN controller presented in this paper is realized on a digital signal processor and its performance is evaluated on the 12-bus flexible ac transmission system benchmark test power system implemented on a real-time platform—the real-time digital simulator. Experimental results show that the DFN controller provides better damping than a conventional linear external controller and requires less SVC reactive power. The damping performance of the DFN controller is also illustrated using transient energy calculations.**

***Index Terms*—Damping controller, dual-function neuron (DFN), real-time digital simulator (RTDS), static var compensator (SVC), wide-area measurements.**

I. Introduction

LARGE power systems, such as the North American Power Grid, have many interconnections and bulk power transmissions over long distances. Due to this, the existing transmission lines are overloaded and have become vulnerable to various faults. The flexible ac transmission system (FACTS) devices, based on power electronics, offer an opportunity to enhance controllability, stability, and power transfer capability of ac transmission systems. A static var compensator (SVC), a shunt FACTS device, has been widely used in power systems for voltage regulation and to increase transient stability in order to increase power transfer. Thus, this allows the transmission line to be compatible with the prevailing load demand [1]. A suitable supplementary external control signal to the SVC voltage control loop can provide damping and improve overall power system stability [2], [3].

A power system containing generators and FACTS devices is a highly nonlinear system. Some conventional methods have been used to design supplementary damping controllers, including the classical pole placement method [4], damping torque analysis [5], linear quadratic Gaussian (LQG) [6], adaptive control [7], etc. In [8] and [9], particle swarm optimization (PSO) is applied to tune the parameters of the SVC external damping controller but based on some linearized mathematical models of power systems. In [10], a neural-network-based controller has been designed for SVC but is based on locally measured signals.

Most of the methods used for designing SVC external damping controllers are based on linear control techniques where the system equations are linearized around a nominal operating point. As the operating conditions change, its performance degrades. Nonlinear controllers using neural networks such as the multilayer perceptron, radial basis function, and Elman network can provide suitable and desired control over a wide range of operating conditions. However, they require long development time and a large number of neurons to deal with complex problems. Their hardware implementations require high-speed processors and a lot of memory. To overcome these drawbacks, a generalized neuron (GN) that requires much smaller training data and time has been reported in [11] for a power system stabilizer design. The GN has a simple structure and its hardware implementation is less expensive.

The use of wide-area measurements provides better understanding of the dynamic behavior of the entire power system. External controllers can be designed using wide-area signals-based models to provide additional damping to power system oscillations. This paper presents the design of two types of external SVC damping controllers using wide-area measurements. The external controllers are specifically designed to enhance the damping in a power system under a wide range of operating conditions. The first type of controller is a linear external damping controller and the second type of controller is a nonlinear external damping controller based on a single dual-function neuron (DFN). The DFN controller design is based on a system identifier called the wide-area monitor (WAM) in this paper. The WAM is realized using two DFN neurons. The entire design is computational efficient in terms of development time and hardware requirements. In addition, the linear and nonlinear external controllers are implemented on a DSP and evaluated on a 12-bus FACTS benchmark test power system [12] which is implemented on the RTDS.

This paper is organized as follows. Section II describes the FACTS benchmark test power system with an SVC studied in this paper. Section III describes the linear external damping controller. Section IV describes the DFN structure and the design of the nonlinear external damping controller. Section V describes the real-time implementation platform and presents some re-

Manuscript received September 2, 2006; revised July 7, 2007. This work was supported by the National Science Foundation under CAREER Grant ECCS # 0348221 and ECCS # 0529292. Paper no. TPWRD-00541-2006.

The authors are with the Real-Time Power and Intelligent Systems Laboratory, Department of Electrical and Computer Engineering, Missouri University of Science and Technology, University of Missouri-Rolla, Rolla, MO 65409-0249 USA (e-mail: gkumar@ieee.org).

Color versions of one or more of the figures in this paper are available online at http://ieeexplore.ieee.org.

Digital Object Identifier 10.1109/TPWRD.2007.916013

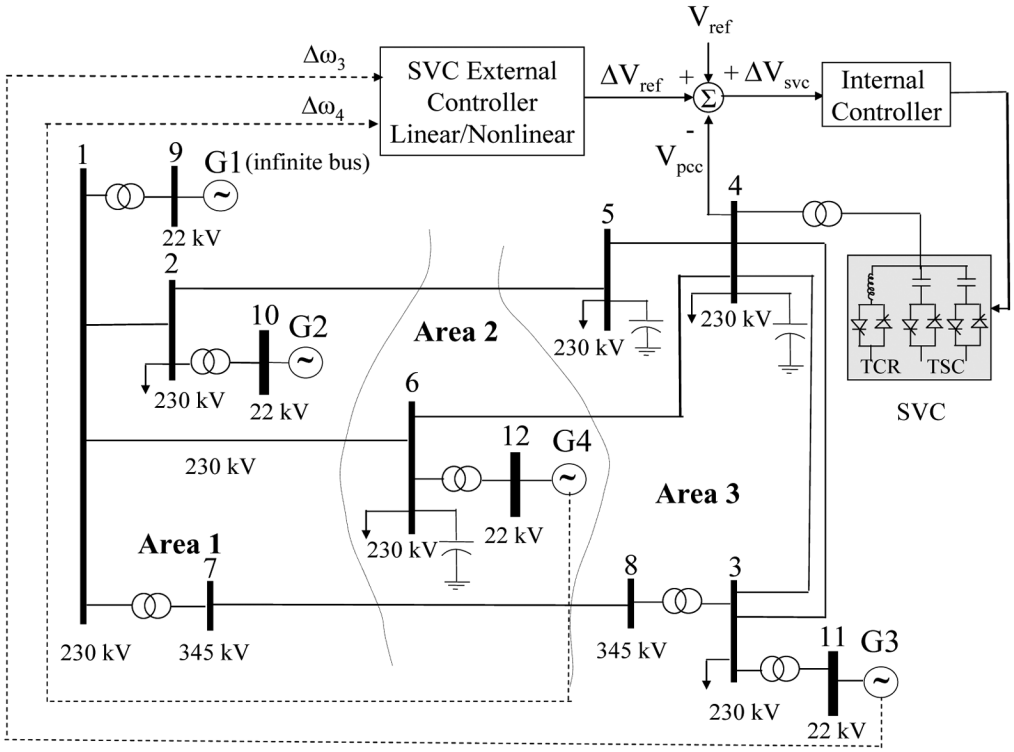

Fig. 1. Twelve-bus FACTS benchmark power system with an SVC external controller.

sults. Section VI presents evaluations and comparisons on the performance of the external controllers based on transient energy calculations. Finally, conclusions and future work are given in Section VII.

II. FACTS Benchmark Test Power System With a Static Var Compensator

The 12-bus FACTS benchmark test power system shown in Fig. 1 consists of six 230-kV buses, two 345-kV buses, and four 22-kV buses [12]. There are three areas in this system consisting of two hydrogenerators—G2 and G4–in areas 1 and 2, respectively, and a thermal generator G3 in area 3 as shown in Fig. 1. The generators are modeled using the detailed synchronous generator models that exist in the RSCAD software with one damper winding on the q axis [13]. The exciter models are IEEE AC1 excitation systems [13]. The parameters of the generators and exciters are given in [12]. This power system is specifically designed to study the applications of FACTS technology. Load-flow and transient stability studies on the test system revealed that it can use FACTS technology for transmission improvements in the following ways [12].

- Install a $\pm$100-MVAr SVC in area 3 at bus 4 to alleviate voltage problems at the load center. Fig. 2 illustrates the effect of the SVC for a 5% increase in load at bus 4 at 2 s. It can be seen that without an SVC, the voltage drops to 0.97 p.u., with a 160-MVAr fixed capacitor, but with an SVC, it is maintained at 0.98 p.u.
- Improvement of transient stability of the system with damping controllers on the SVC and other FACTS devices.

To avoid system instability during large disturbances, the authors have added governor–turbine models to the hydrogenerators in areas 1 and 2, and to the thermal generator in area 3. The hydro–governor and IEEE Type 1 governor RSCAD models, respectively, are used [13]. Parameters of the governors and the turbines are given in [14].

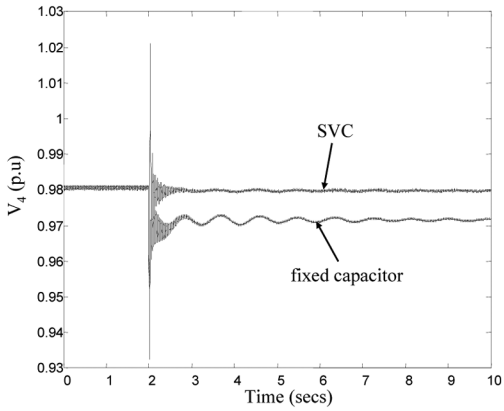

Fig. 2. Comparison of bus 4 voltage response for a 5% increase in the load at bus 4 at $t = 2$ s with a fixed capacitor (160 MVAr) and an SVC ($\pm$100 MVAr).

III. Linear External Damping Controller

A conventional linear external damping controller similar to the structure presented in [15] as shown in Fig. 3 has been designed for the SVC and implemented on the RTDS in this paper. The inputs to this controller are speed deviations of generators G3 and G4 which are based on wide-area measurements. The controller output is $\Delta V_{\rm ref}$ which is added to the SVC internal controller reference $V_{\rm ref}$. The SVC internal controller is a proportional-integral (PI) controller. The objective when selecting the PI parameters is to have a wide stable operating region as much as possible around a nominal operating point.

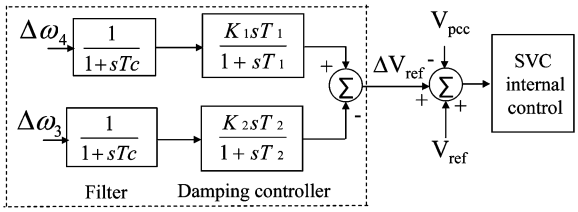

Fig. 3. Linear external damping controller for an SVC.

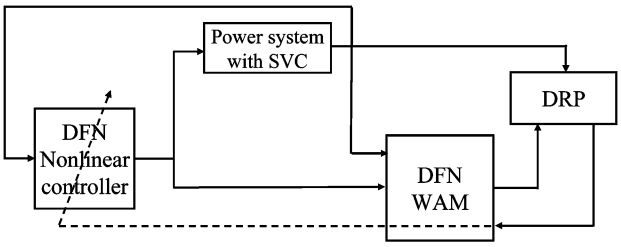

Fig. 4. Indirect adaptive control method-based DFN controller for SVC.

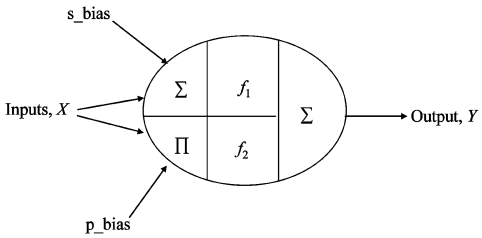

Fig. 5. DFN model.

Hence, a nonlinear external controller is required for optimal performance at various operating regions to provide a change in $V_{\rm ref}$ for the internal controller. A 200-ms three-phase short-circuit fault is applied halfway between buses 7 and 8 and the parameters of the damping controllers are tuned for this disturbance to obtain the best performance based on time-response analysis (minimum overshoots and faster settling time) [16]. The parameters obtained are $K_1 = 5.0$; $T_1 = 1.0$; $K_2 = 15.0$; and $T_2 = 0.05$.

IV. Nonlinear External Damping Controller

The design of the nonlinear damping controller is based on the indirect adaptive control method as shown in Fig. 4 [17], consisting of a DFN power system dynamics identifier, the WAM, and a DFN controller. Section IV-A–D describes the DFN structure, the particle swarm optimization algorithm used in determining the parameters of the DFNs, WAM, the desired response predictor (DRP), and the DFN nonlinear controller.

A. Dual-Function Neuron

A common neuron model consists of a sigmoidal threshold function and an ordinary summation or product as aggregation functions whereas a DFN has fuzzy compensatory operators as aggregation operators [18]. The structure of a DFN is shown in Fig. 5.

For a network with a single output, the size of a conventional neural network, such as the multilayer perceptron (MLP) is $n \times m \times 1$ whereas the size of a DFN is $n \times 2 \times 1$ where n and m are the number of input and hidden neurons, respectively. This means that the MLP has $(n \times m) + (m \times 1)$ weights whereas the DFN has $2n+1$ weights. Comparing the number of weights in both cases, for a single output network, the MLP has a large number of weights compared to a DFN. Due to fewer weights and fuzzy aggregation operators, a DFN has a shorter training time and less hardware requirements. In addition, the DFN has good fault-tolerant capabilities for any complex problem.

The output of the first $\sum$ in Fig. 5 with an activation function f_1 is given as

$$O_{\sum} = f_1(s\_net) \tag{1}$$

$$\text{where } s\_net = \sum W_{\sum} X + X_{o\sum} \tag{2}$$

where $W\sum$ is the weight for the input X, and $X_{o\sum}$ is the bias applied to $\sum_1$. The output of the $\prod$ part with the activation function f_2 is given as

$$O_{\prod} = f_2(pi\_net) \tag{3}$$

$$\text{where } pi\_net = \prod W_{\prod} X + X_{o\prod} \tag{4}$$

where $W_{\prod}$ is the weight for the input X, and $X_{o\prod}$ is the bias applied to $\prod$ part. The final output Y of the neuron is a function of the two outputs of $O_{\sum}$ and $O_{\prod}$ with the weights W and $(1-W)$, respectively [11], and is given as

$$Y = O_{\prod} \times (1 - W) + O_{\sum} \times W. \tag{5}$$

Thus, for any application, only three types of weights $W\Sigma$, $W\prod$, and W need to be determined with the DFN structure. The PSO algorithm has been reported to be an excellent algorithm for training neural networks [19] and, therefore, it is used to determine the DFN weights in this paper.

B. DFN Training Using PSO

The PSO algorithm is a population-based search algorithm, based on the simulation of the social behavior of birds within a flock. A swarm consists of a set of particles, where each particle represents a potential solution with parameters in d dimensions. The dimension d corresponds to the number of weights in the DFN. The changes to the position of a particle (ith particle) and its operation in a swarm are influenced by the experience and the knowledge of its neighbors. The position $x_{id}(k+1)$ of the ith particle in the dth dimension at instant $(k+1)$ is given as

$$\begin{aligned} x_{id}(k+1) = {} & x_{id}(k) + w \times v_{id}(k) \\ & + c_1 \times \mathrm{rand}_1 \times (\mathrm{p_{id}(k)} - \mathrm{x_{id}(k)}) \\ & + c_2 \times \mathrm{rand}_2 \times (\mathrm{p_{gd}(k)} - \mathrm{x_{id}(k)}) \end{aligned} \tag{6}$$

where $v_{id}(k)$ is the velocity of the ith particle in the dth dimension at instant k, $p_{id}(k)$ is the pbest—the position where the ith particle has found the highest fitness over k instants, $p_{gd}(k)$ is the gbest of the swarm—the position of the particle in the swarm with the highest fitness over k instants, and rand_1 and rand_2 are uniform random numbers between 0 and 1. The following PSO

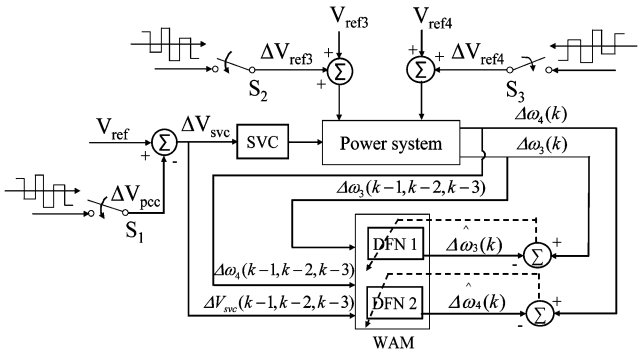

Fig. 6. Training of WAM with PRBS applied.

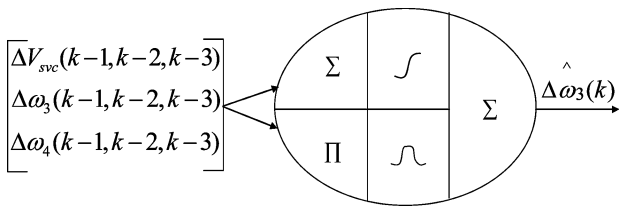

Fig. 7. WAM DFN 1 structure estimating the speed deviation of generator G3.

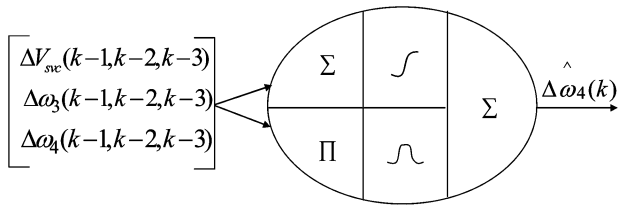

Fig. 8. WAM DFN 2 structure estimating the speed deviation of generator G4.

parameters, commonly used in PSO applications [19], are used in this paper.

- Maximum search space range (−100,100).
- Inertia constant w 0.8.
- Acceleration constants c_1, $c_2$2, 2.
- Number of PSO particles 25.

C. Wide-Area Monitor (WAM)

As a first step toward designing the nonlinear controller, a WAM is designed using a DFN. A WAM provides a model of the system at every time instant to the controller so that appropriate control signals can be generated. As shown in Fig. 6, the inputs to the WAM are time delayed values $(k-1)$, $(k-2)$, $(k-3)$, of the speed deviations of generators $G3(\Delta\omega_3)$ and $G4(\Delta\omega_4)$, and the voltage reference ΔV_{SVC}, all sampled at 125 Hz. The outputs of the WAM are the estimated speed deviations of generators G3 and G4 at time instant k. The WAM is realized using two separate DFNs. Figs. 7 and 8 show the DFN 1 and DFN 2 for estimating generator G3 and G4 speed deviations, respectively.

As shown in Fig. 6, constant excitation voltage references $V_{\rm ref3}$ and $V_{\rm ref4}$ are applied to the generators G3 and G4, respectively, at a particular steady-state operating point. The WAM is trained by adding pseudorandom binary signals (PRBS), $\Delta V_{\rm ref3}$, $\Delta V_{\rm ref4}$, and $\Delta V_{\rm pcc}$ to generator G3, generator G4, and at the SVC point of common coupling (PCC) (i.e., bus 4, respectively). These signals provide $\pm 10\%$ deviations in the steady-state values of$V_{\rm pcc}$, $V_{\rm ref3}$, and $V_{\rm ref4}$. The PRBS signals applied to generator excitations are square waves of frequencies 5, 3, and 2 Hz and that applied to the SVC are square waves of frequencies 0.5, 0.3, and 0.2 Hz. The PRBS signals are applied to the power system by closing switches S_1, S_2, and S_3 as shown in Fig. 6. WAM is trained offline using the PSO algorithm.

In DFN 1 and DFN 2, sigmoidal functions (f_1) are used with the $\sum$ summation aggregation function while Gaussian functions (f_2) are used with the $\prod$ product aggregation function as given in (7) and (8)

$$f_1(\text{s\_net}) = \frac{1}{1+e^{(-0.01s\_net)}} \tag{7}$$

$$f_2(\text{pi\_net}) = e^{(-0.01\text{pi\_net}^2)}. \tag{8}$$

Thus, there is flexibility at both the aggregation and the threshold level in a DFN and so it is better equipped to model the nonlinearities involved in the power system than just a single functional neuron or neural network. Each DFN has a size of $9 \times 2 \times 1$ and, thus, a total of 19 weights.

D. Nonlinear DFN Controller and DRP

The DFN controller is designed based on the indirect adaptive control method as shown in Figs. 4 and 9. Once the WAM is able to estimate the speed deviations of the generators G3 and G4 in the power system, the nonlinear controller can be developed. The DFN controller (Fig. 10) consists of a sigmoidal function (f_1) used with the $\sum$ summation aggregation function and a Gaussian function (f_2) used with the $\prod$ product aggregation function as given in (9) and (10). The inputs to the DFN controller are speed deviations of generators G3 and G4 and $\Delta V_{\rm svc}$, at time instants $(k-1)$, $(k-2)$, $(k-3)$, and the output is the external damping signal applied to the SVC, the deviation in voltage reference $\Delta V_{\rm ref}$ at time instant k. The DFN controller has a total of 19 weights

$$f_1(\text{s\_net}) = \frac{1}{1+e^{(-\text{s\_net})}} \tag{9}$$

$$f_2(\text{pi\_net}) = e^{(-\text{pi\_net}^2)}. \tag{10}$$

Fig. 9 shows the schematic diagram illustrating the training of the DFN controller. Here, the inputs to the trained WAM are given at time instants k, $(k-1)$, $(k-2)$, and speed deviations of generators G3 and G4 at time instant $(k+1)$ are estimated. A DRP is also used to estimate the speed deviations at time instant $(k+1)$. More details on the design of the DRP are given in [17]. The DRP equations used in the DFN controller design in Fig. 9 are given in (11) and (12)

$$\begin{aligned}\Delta\omega 3_{\rm DRP}(k+1) = {} & 0.01 \times (0.4\Delta\omega_3(k) + 0.4\Delta\omega_3(k-1) \\ & + 0.16\Delta\omega_3(k-2))\end{aligned} \tag{11}$$

$$\begin{aligned}\Delta\omega_{4_{\rm DRP}}(k+1) = {} & 0.01 \times (0.4\Delta\omega_4(k) + 0.4\Delta\omega_4(k-1) \\ & + 0.16\Delta\omega_4(k-2)).\end{aligned} \tag{12}$$

All the poles of the DRP lie on the left-hand side of the s-plane which implies that the DRP system is stable and the dominant poles are -2.0417 and $(-2.1979 \pm 2.1730i)$.

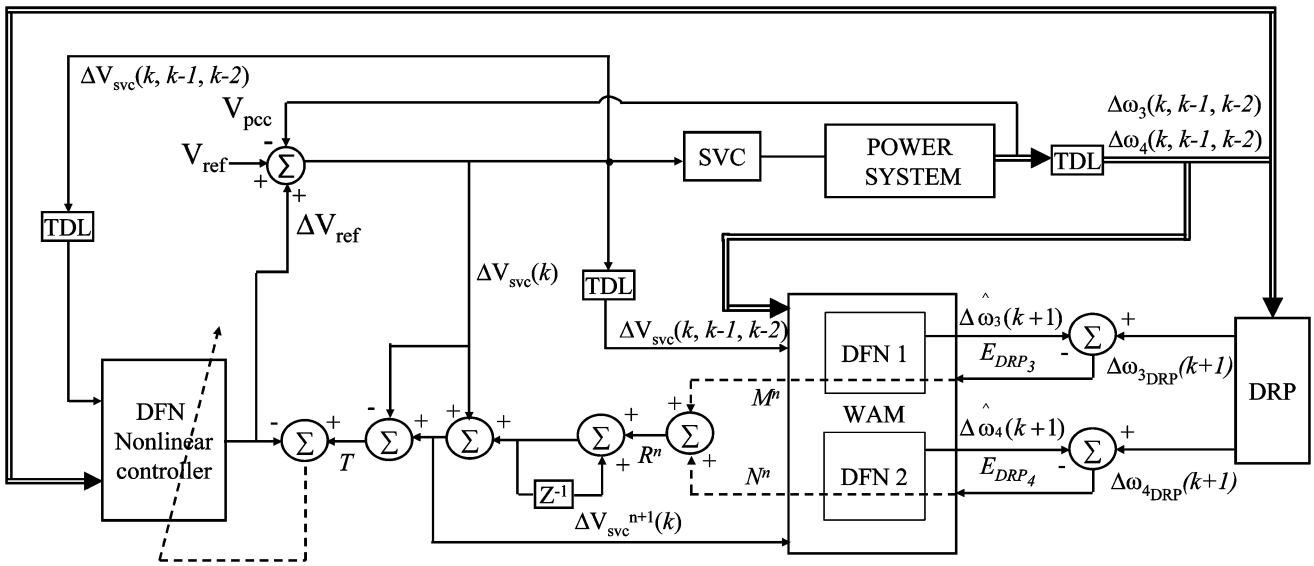

Fig. 9. Schematic diagram illustrating the training of the DFN nonlinear controller.

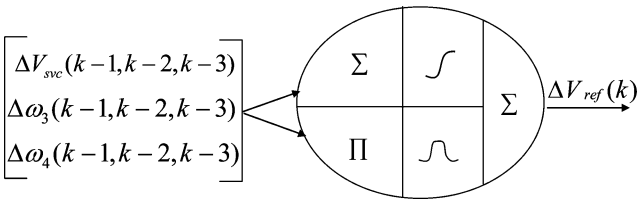

Fig. 10. DFN structure for the nonlinear controller.

The difference between the outputs of DRP and the WAM [(13) and (14)] are used to obtain the target T for the output of the DFN controller as shown in Fig. 9. The sum-squared errors in (15) are minimized by adapting the weights of the DFN controller.

$$E_{\mathrm{DRP}_3} = [(\Delta\hat{\omega}_3(k+1) - \Delta\omega_{3_{\mathrm{DRP}}}(k+1)] \quad (13)$$

$$E_{\mathrm{DRP}_4} = [(\Delta\hat{\omega}_4(k+1) - \Delta\omega_{4_{\mathrm{DRP}}}(k+1)] \quad (14)$$

$$E_3 = 0.5E^2_{\mathrm{DRP}_3} \text{ and } E_4 = 0.5E^2_{\mathrm{DRP}_4}. \quad (15)$$

The error signals E_{DRP3} and E_{DRP4} are backpropagated through DFN 1 and DFN 2 of the WAM through to the input ΔV_{svc} to obtain the signals M and N, respectively, as shown in Fig. 9. The mathematical representation of the signals obtained at M and N is given in (16) and (17), respectively

$$M = \frac{\partial E_{\mathrm{DRP3}}(k+1)}{\partial \Delta V_{\mathrm{svc}}(k)} = E_{\mathrm{DRP}_3}((W_1 \cdot O_{\sum_1} \cdot (1 - O_{\sum_1}) \cdot W_{\sum_{1\Delta V_{\mathrm{svc}}(k)}})) + \frac{((1-W_1)\cdot(-2)\cdot \mathrm{pi\_net}_1 \cdot O_{\prod_1} \cdot \mathrm{pi\_net}_1}{\Delta V_{\mathrm{svc}}(k))} \quad (16)$$

$$N = \frac{\partial E_{\mathrm{DRP4}}(k+1)}{\partial \Delta V_{\mathrm{svc}}(k)} = E_{\mathrm{DRP}_4}((W_2 \cdot O_{\sum_2} \cdot (1 - O_{\sum_2}) \cdot W_{\sum_{2\Delta V_{\mathrm{svc}}(k)}})) + \frac{((1-W_2)\cdot(-2)\cdot \mathrm{pi\_net}_2 \cdot O_{\prod_2} \cdot \mathrm{pi\_net}_2}{\Delta V_{\mathrm{svc}}(k))} \quad (17)$$

where, the subscript "1" refers to the variables of DFN 1 and subscript "2" refers to the variables of DFN 2. $W_{\sum_1 \Delta V_{\mathrm{svc}}(k)}$ and $W_{\sum_2 \Delta V_{\mathrm{svc}}(k)}$ are weights $W_{\sum}$ with respect to the input $\Delta V_{\mathrm{svc}}(k)$ of DFN 1 and DFN 2, respectively. Other variables are defined in Section IV-A.

The signals M and N are added to obtain the signal R as shown in (18). For a given set of values of speed deviations of generators G3 and G4 at time instant k, the signal ΔV_{svc} is updated n times as shown in (19), each time with R^n, in order to minimize the errors E_{DRP3} and E_{DRP4} given in (13) and (14), respectively. By doing so, the signal T, given in (20), is the exact target signal required to minimize the errors given by (13) and (14) at time instant k. This process is repeated for each value of input $\Delta V_{\mathrm{svc}}(k)$. In this study, n is chosen to be 5 because E_{DRP3} and E_{DRP4} are considerably minimized at the end of the fifth iteration

$$R^n = M^n + N^n \quad (18)$$

$$\Delta V^{i+1}_{\mathrm{svc}}(k) = R^n + \Delta V^i_{\mathrm{svc}}(k) \quad \text{for } i = 1, \ldots, n \quad (19)$$

$$T = \Delta V^{n+1}_{\mathrm{svc}}(k) - \Delta V_{\mathrm{svc}}(k) \quad (20)$$

where $\Delta V_{\mathrm{svc}}(k) = V_{\mathrm{ref}}(k) + \Delta V_{\mathrm{ref}}(k) - \Delta V_{\mathrm{pcc}}(k)$.

The mean-squared error between the DFN controller output and the target T signal is minimized by updating the DFN controller weights using the PSO algorithm.

V. Real-Time Implementation and Results

A. Real-Time Digital Simulator (RTDS)

Due to the complexity and expensive nature of the power system, it is very difficult to test new control methods and algorithms on the real-world power system. The RTDS is a fully digital power system simulator capable of continuous real-time operation. It performs electromagnetic transient power system simulations with a typical time step of 50 μs utilizing a combination of custom software and hardware. The proprietary operating system used by the RTDS guarantees "hard real time"

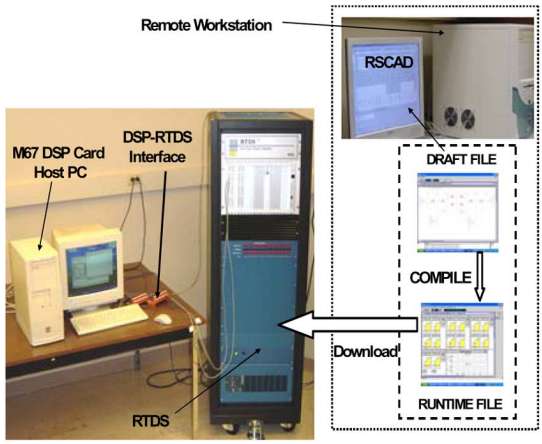

Fig. 11. Laboratory hardware setup with RTDS.

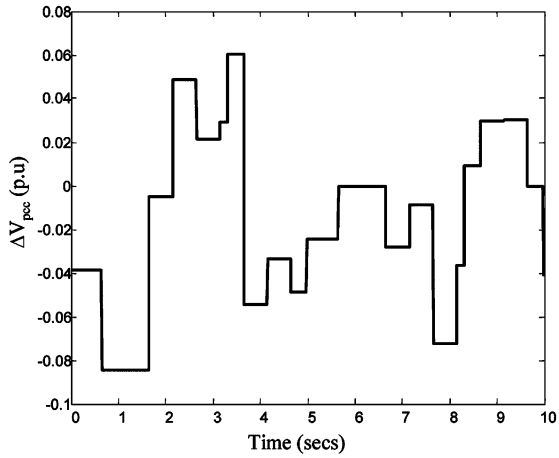

Fig. 12. PRBS applied to the excitation system of generator G3 $\Delta V\mathrm{ref}_3$.

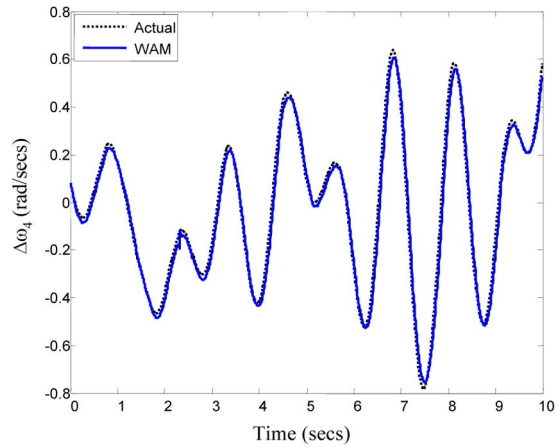

Fig. 13. Actual and WAM estimation of speed deviation of generator G4 for the PRBS in Fig. 12 applied.

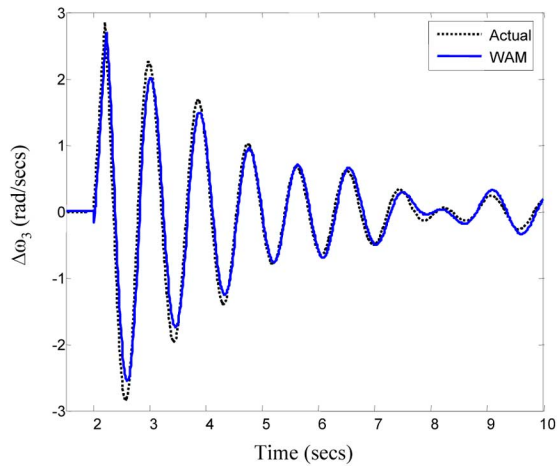

Fig. 14. Actual and WAM estimation of speed deviation of generator G3 during a transmission-line outage between buses 4 and 5 in Fig. 1.

during all simulations [20]. It is an ideal tool for the design, development, and testing of power system protection and control designs.

The performances of the linear and nonlinear external damping controllers are evaluated on the 12-bus FACTS benchmark test power system implemented on the RTDS. The WAM and nonlinear controller are implemented on a digital signal processor (DSP) which is interfaced to the RTDS that runs the power system. The nonlinear controller is trained offline (this means that the DFN output is not added to the SVC internal controller reference during the development) and is implemented on the Innovative Integration M67 DSP card which is equipped with analog/digital converter modules (A4D4) [21]. The DSP and RTDS interface and laboratory hardware setup is shown in Fig. 11. More details on the laboratory setup are given in [22].

B. Experimental Results

This section presents experimental results of the WAM and the linear and nonlinear external controllers. The damping performances of the linear and nonlinear controllers are compared.

1) WAM: After the WAM DFNS are trained, it is tested under small and large disturbances—PRBS signals and short-circuit faults, respectively. Fig. 12 shows a typical PRBS signal applied to the excitation system of generator G3. The PRBS signals provide $\pm 10\%$ deviations in the reference voltages of excitations of generators G3, G4, and reference voltage at the SVC PCC. This disturbance is chosen to be small because, in a real power system, applying large magnitude perturbations to the network might not be desirable or practical. This shows that a DFN can be trained on a real power system with small perturbations applied. Fig. 13 shows the corresponding speed deviation of generator G4.

Now a large disturbance is carried out and tested to see whether the WAM can predict the speed deviations. Fig. 14 shows speed deviation of generator G3 and output of WAM for a permanent transmission-line outage between buses 4 and 5 in Fig. 1. It can be seen that WAM predicts the speed deviations of generators G3 and G4 accurately for different disturbances.

2) Linear External Damping Controller: To illustrate the effect of an external damping controller, a 200-ms three-phase short circuit is applied at bus 7. Figs. 15 and 16 show the speed deviations of generators G3 and G4, respectively, with and without a linear external damping controller to the SVC (Fig. 1). It can be clearly seen that the damping is improved with the linear external controller.

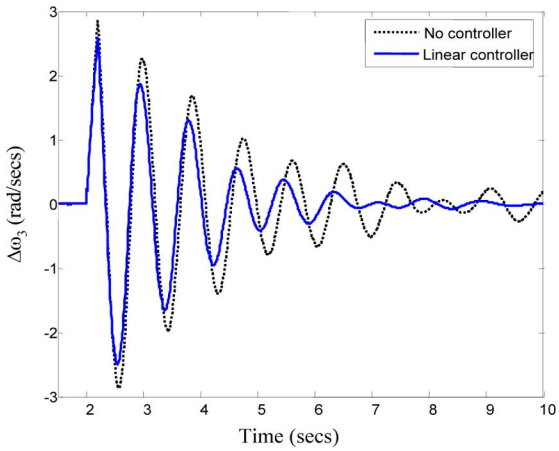

Fig. 15. Speed deviation of generator G3 with and without a linear controller during a 200-ms three-phase short-circuit fault applied at bus 7.

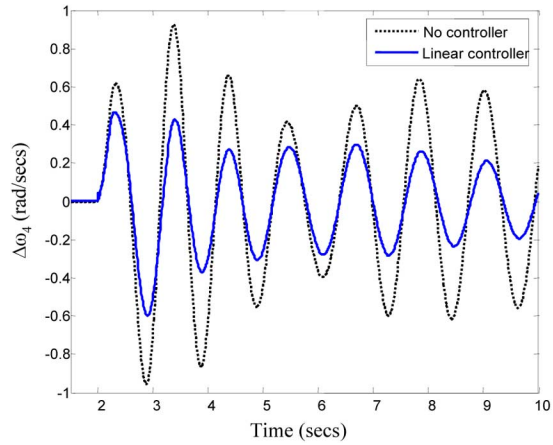

Fig. 16. Speed deviation of generator G4 with and without a linear controller during a 200-ms three-phase short-circuit fault applied at bus 7.

3) Comparison of Linear and Nonlinear Controllers: Several tests are carried out to evaluate the performance of linear and nonlinear external damping controllers for power system oscillations damping. Four of these tests are described below.

Test 1: This test is carried out to evaluate and compare the performances of two controllers. Results are given for a system without an external controller. The system is subjected to a 200-ms three-phase short circuit applied at bus 3. Figs. 17 and 18 show the speed deviations of generator G3 and G4, respectively, for this fault. It can be seen that the nonlinear controller damps out the speed oscillations faster than the linear controller.

Test 2: This test is carried out to show that the nonlinear controller provides better damping than the linear controller. A 200-ms three-phase short circuit is applied now at bus 5. Figs. 19 and 20 show the speed deviations of generators G3 and G4 for this fault. It can be seen that the nonlinear controller damps the speed oscillations faster than the linear controller.

Test 3: A permanent transmission-line outage is carried out between buses 4 and 5. Figs. 21 and 22 show the speed deviations of generators G3 and G4. It can be seen that the nonlinear controller damps the speed oscillations faster than the linear controller. Fig. 22 shows that the nonlinear controller damps the speed oscillations of generator G4 in about 7 s, injecting less transient energy into the system whereas the linear controllers do not damp the oscillations completely until after 10 s.

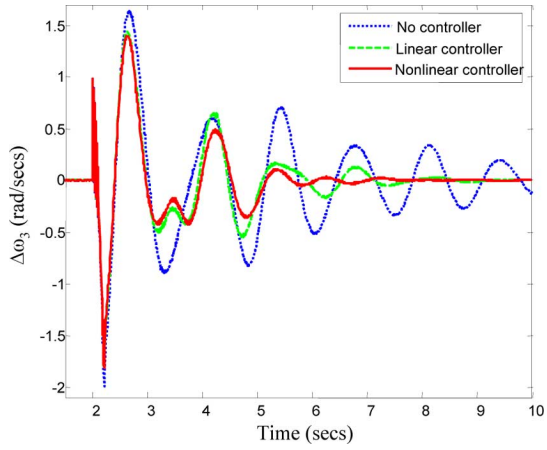

Fig. 17. Speed deviation of generator G3 for a 200-ms three-phase short-circuit fault applied at bus 3.

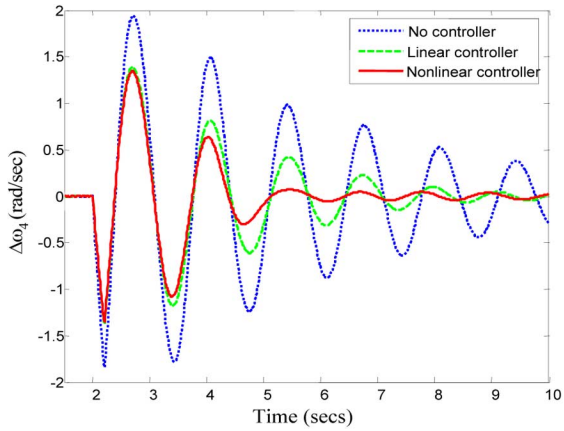

Fig. 18. Speed deviation of generator G4 for a 200-ms three-phase short-circuit fault applied at bus 3.

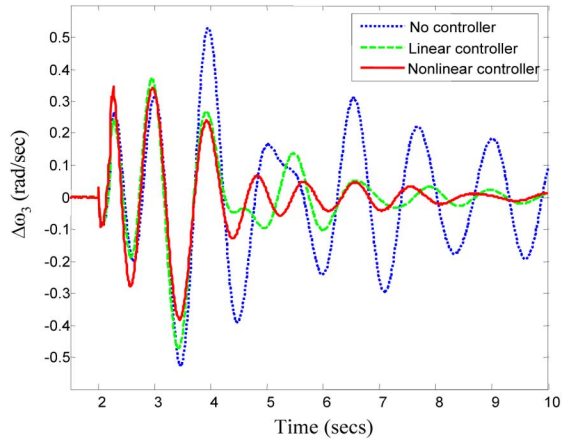

Fig. 19. Speed deviation of generator G3 for a 200-ms three-phase short-circuit fault applied at bus 5.

Test 4: Fig. 23 shows the speed deviations of generator G4 for a permanent transmission-line outage between buses 2 and 5.

It can be seen that the linear controller oscillates until the end of 10 s whereas the nonlinear controller damps the oscillations at about 8 s. It can be seen from Figs. 24 and 25 that the SVC, when

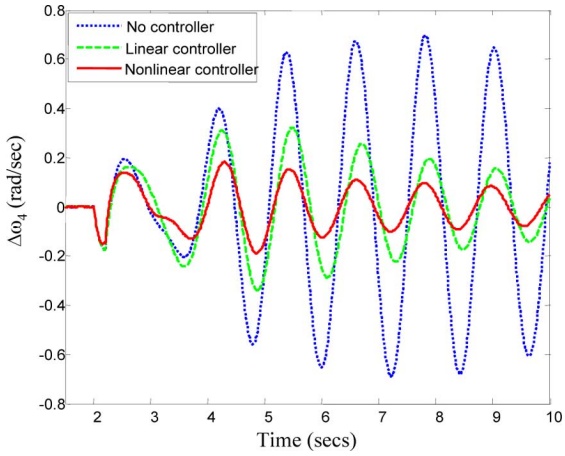

Fig. 20. Speed deviation of generator G4 for a 200-ms three-phase short-circuit fault applied at bus 5.

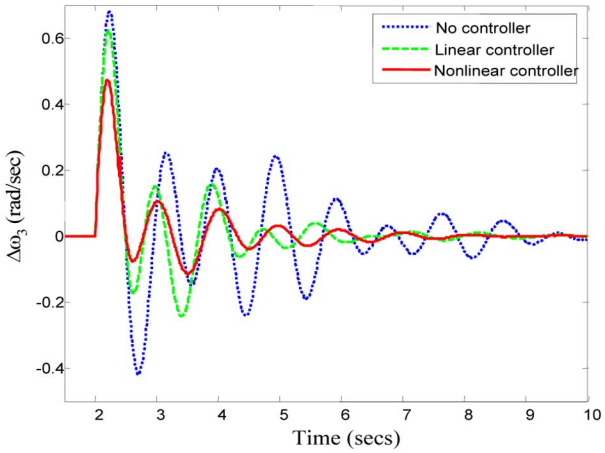

Fig. 21. Speed deviation of generator G3 for a permanent transmission-line outage between buses 4 and 5.

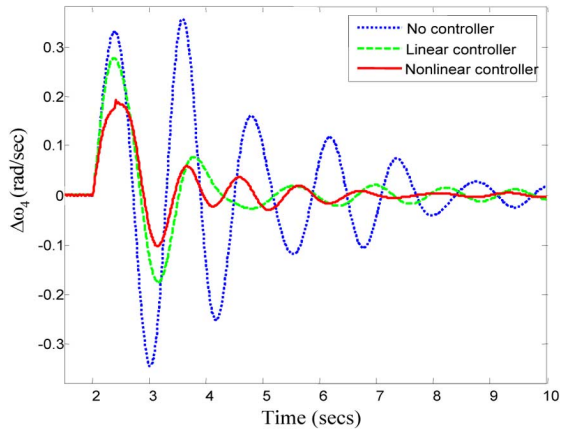

Fig. 22. Speed deviation of generator G4 for a permanent transmission-line outage between buses 4 and 5.

externally controlled by the nonlinear controller, injects less reactive power and provides better performance. This means that with nonlinear intelligent control, the capacity/sizing of an SVC that is required is smaller which translates to reduced cost and installation space. It can be seen in Fig. 25 that due to the transmission-line outage, there is a change in operating conditions

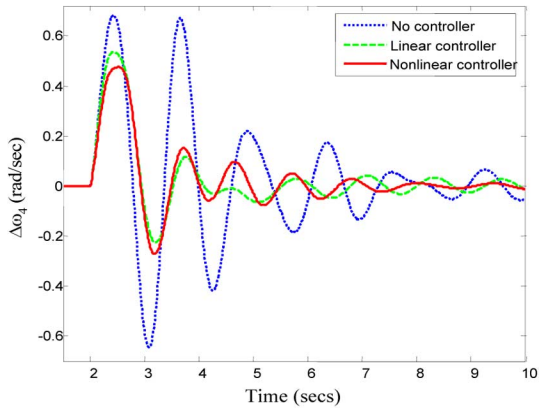

Fig. 23. Speed deviation of generator G4 for a transmission-line outage between buses 2 and 5.

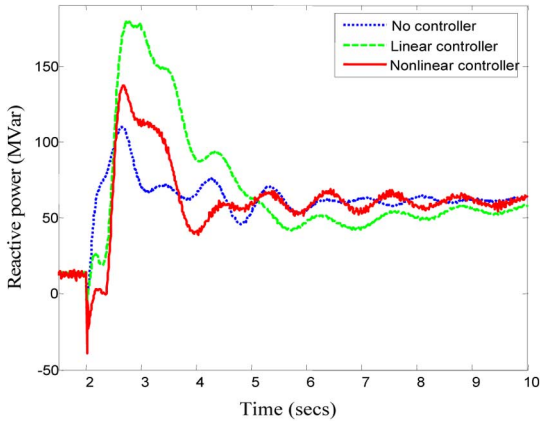

Fig. 24. Reactive power injected by linear and nonlinear controllers for Test 4.

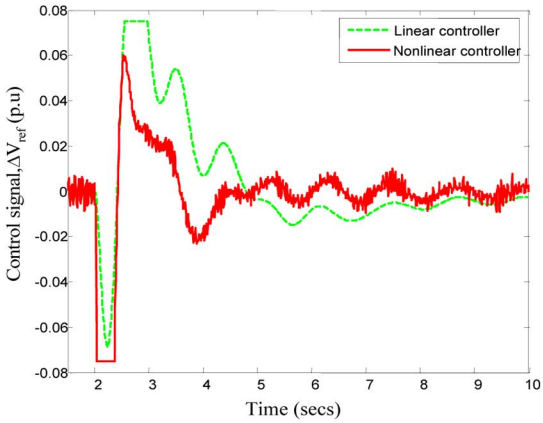

Fig. 25. Control signals injected by linear and nonlinear controllers for Test 4.

and the linear controller response has become slower which is not desirable, whereas the nonlinear controller responds quickly and injects the control signals in such a way that it changes the reference voltage to damp out the system oscillations. The linear and nonlinear external controller output signals are limited to ± 0.075 p.u. in all of these tests.

VI. Discussions

The performance of the linear and nonlinear controllers is evaluated in this section in terms of the transient energies. When

TABLE I
NORMALIZED PERFORMANCE INDICES OF THE LINEAR AND NONLINEAR CONTROLLER FOR SPEED DEVIATIONS OF GENERATOR G3

	Test 1	Test 2	Test 3	Test 4	Overall
No controller	1.0	1.0	1.0	1.0	1.0
Linear controller	1.57	1.86	1.97	2.03	1.86
Nonlinear controller	1.86	2.13	4.45	2.8	2.81

TABLE II
NORMALIZED PERFORMANCE INDICES OF THE LINEAR AND NONLINEAR CONTROLLER FOR SPEED DEVIATIONS OF GENERATOR G4

	Test 1	Test 2	Test 3	Test 4	Overall
No controller	1.0	1.0	1.0	1.0	1.0
Linear controller	2.39	1.73	3.23	3.17	2.63
Nonlinear controller	3.02	5.13	6.62	3.46	4.56

a disturbance occurs in a power system, the transient energy injected into the system can cause it to go unstable if the controllers do not provide sufficient damping. Therefore, a robust damping controller is required to minimize the transient energy injected into the system for various disturbances.

For the tests carried out in Section V, the transient energies of generators G3 and G4 within the first 3 s after the disturbances are calculated [$t_f - t_s = 3$ s, given in (22)] for: 1) without an external controller, 2) with a linear controller, and 3) with a nonlinear controller

$$T.E_G = \sum_{t=t_s}^{t_f} 0.5^* H_G^* \Delta\omega_G^2 \tag{22}$$

where G is the generator G3 or G4; H is the inertia constant of generator G; and $\Delta\omega_G$ is the speed deviation of generator G.

The performance of the linear and the nonlinear controllers is compared by defining a performance index (P.I) given in (23)

$$P.I = \frac{1}{T.E_G}. \tag{23}$$

Tables I and II show the performance comparisons of the linear and nonlinear controllers in terms of the transient energies of generators G3 and G4, respectively. The P.Is are normalized by dividing the P.Is by that P.I obtained without an external controller.

In Table I, it can be seen that the overall performance of the nonlinear controller in terms of transient energy of generator G3 is 2.81 times better than the system without an external controller whereas the overall performance of the linear controller is 1.86 times better than the system without an external controller. Similarly, it can be seen from Table II that the overall performance of nonlinear controller in terms of transient energy of generator G4 is 4.56 times better than the system without an external controller whereas the linear controller is 2.63 times better than the system without an external controller. Thus, the SVC external controllers have greater damping on the system.

VII. CONCLUSION

The design and real-time implementation of a single DFN-based nonlinear external damping controller for an SVC has been presented. A DFN-based WAM has been developed to identify the power system dynamics. The inputs to the WAM and external controllers are based on wide-area measurements. The performance of a DFN-based nonlinear controller has been compared with a conventional linear external damping controller and shown to be better. This is as a result of the WAM, which provides accurate system dynamics information from moment to moment and, thus, better control is realized.

Experimental results are presented to show that WAM identifies the system dynamics correctly and the nonlinear DFN controller provides better damping to the system oscillations. Various other results show that the nonlinear controller provides better damping with less reactive power injection. The nonlinear controller has a higher performance index which implies that it injects less transient energy during a disturbance which ensures that the system remains stable for various disturbances.

The number of weights with DFN is almost an order less for implementation than with standard neural-network structures, such as the MLPs. Therefore, the major advantage of the DFN-based control architecture is that it requires shorter training time and can still exhibit robust performance. Hence, combining benefits of DFN and wide-area measurements not only helps to design a good controller but also makes it easier to implement it in real time. Future work involves developing the PSO to be computationally efficient for online adaptation of the parameters of the DFNs in the WAM and in the nonlinear controller.

REFERENCES

[1] N. G. Hingorani and L. Gyugi, *Understanding FACTS, Concepts and Technology of Flexible AC Transmission Systems*. Piscataway, NJ: IEEE Press, 2000.
[2] C. J. Wu and Y. S. Lee, "Damping of synchronous generator by static reactive power compensator with digital controller," in *Proc. Inst. Elect. Eng., Gen., Transm. Distrib.*, 1991, pp. 18–24.
[3] E. N. Lerch, D. Povh, and L. Xu, "Advanced SVC control for damping power system oscillations," *IEEE Trans. Power Syst.*, vol. 6, no. 2, pp. 524–535, May 1991.
[4] P. Kundur, *Power System Stability and Control*. New York: McGraw-Hill, 1993.
[5] K. R. Padiyar and R. K. Varma, "Damping torque analysis of static var system controllers," *IEEE Trans. Power Syst.*, vol. 6, no. 2, pp. 458–465, May 1991.
[6] J. R. Smith, D. A. Pierre, D. A. Rudberg, and A. P. Johnson, "An enhanced LQ adaptive var unit controller for power system damping," *IEEE Trans. Power Syst.*, vol. 4, no. 2, pp. 443–451, May 1989.
[7] J. R. Smith, D. A. Pierre, I. Sadighi, M. H. Nehrir, and J. F. Hauer, "A supplementary adaptive var unit controller for power system damping," *IEEE Trans. Power Syst.*, vol. 4, no. 3, pp. 1017–1023, Aug. 1989.
[8] T. Okada, T. Watanabe, and K. Yasuda, "Parameter tuning of fixed structure controller for power system stability enhancement," in *Proc. Inst. Elect. Eng., Transm. Distrib. Conf. Exhibit.*, Asia Pacific, 2002, vol. 1, pp. 162–167.
[9] S. M. Bamasak and M. A. Abido, "Assessment study of shunt FACTS based controllers effectiveness on power system stability enhancement," in *Inst. Elect. Eng., Univ. Power Eng. Conf.*, 2004, vol. 1, pp. 274–278.

[10] B. Changaroon, S. C. Srivastava, D. Thukaram, and S. Chirarattananon, "Neural network based power system damping controller for SVC," *Proc. Inst. Elect. Eng., Gen. Transm. Distrib.*, vol. 146, no. 4, pp. 370–376, 1999.
[11] D. K. Chaturvedi, O. P. Malik, and P. K. Kalra, "Generalised neuron-based adaptive power system stabilizer," *Proc. Inst. Elect. Eng., Gen. Transm. Distrib.*, vol. 151, pp. 213–218, 2004.
[12] S. Jiang, U. D. Annakkage, and A. M. Gole, "A platform for validation of FACTS models," *IEEE Trans. Power Del.*, vol. 21, no. 1, pp. 484–491, Jan. 2006.
[13] "RSCAD User's Guide, Version 1.204" RTDS Technologies, Inc., Winnipeg, MB, Canada. [Online]. Available: www.rtds.org.
[14] J. Sandhya and G. K. Venayagamoorthy, "Identification of SVC dynamics using wide area signals in a power system," presented at the IEEE Power Eng. Soc. General Meeting, 2006.
[15] J.-W. Park, R. G. Harley, and G. K. Venayagamoorthy, "New external neuro-controller for series capacitive reactance compensator in a power network," *IEEE Trans. Power Syst.*, vol. 19, no. 3, pp. 1462–1472, Aug. 2004.
[16] K. Ogata, *Modern Control Engineering*. Upper Saddle River, NJ: Prentice-Hall, 1996.
[17] G. K. Venayagamoorthy and R. G. Harley, "Two separate continually online-trained neurocontrollers for excitation and turbine control of a turbogenerator," *IEEE Trans. Ind. Appl.*, vol. 38, no. 3, pp. 887–893, May/Jun. 2002.
[18] M. Mizumoto, "Pictorial representations of fuzzy connectives," *Fuzzy Sets Syst.*, vol. 32, pp. 45–79, 1989.
[19] V. G. Gudise and G. K. Venayagamoorthy, "Comparison of particle swarm optimization and backpropagation as training algorithms for neural networks," in *Proc. IEEE Swarm Intelligence Symp.*, Indianapolis, IN, 2003, pp. 110–117.
[20] P. Forsyth, T. Maguire, and R. Kuffel, "Real time digital simulation for control and protection system testing," in *Proc. IEEE 35th Annu. Power Electronics Specialistis Conf.*, 2004, vol. 1, pp. 329–335.
[21] "OMNIBUS User's Manual," Innovative Integration, CA, 2001.
[22] G. K. Venayagamoorthy and S. Ray, "A neural network based optimal wide area scheme for a power system," in *Proc. Industry Applications Conf.*, Oct. 2005, vol. 1, pp. 700–706.

Ganesh Kumar Venayagamoorthy (S'91–M'97–SM'02) received the B.Eng. degree (Hons.) in electrical and electronics engineering from Abubakar Tafawa Balewa University, Bauchi, Nigeria, in 1994, and the M.Sc.Eng. and Ph.D. degrees in electrical engineering from the University of Natal, Durban, South Africa, in 1999 and 2002, respectively.

He was a Senior Lecturer with the Durban Institute of Technology, Durban, prior to joining the Missouri University of Science and Technology, Rolla (Missouri S & T), in 2002. Currently, he is an Associate Professor of Electrical and Computer Engineering and Director of the Real-Time Power and Intelligent Systems Laboratory at Missouri S & T. He was a Visiting Researcher with ABB Corporate Research, Sweden, in 2007. His research interests are the development and applications of computational intelligence for real-world applications, including power systems stability and control, FACTS devices, power electronics, alternative sources of energy, sensor networks, collective robotic search, signal processing, and evolvable hardware. He has published books, book chapters, refereed journals papers, and refereed international conference proceeding papers.

Dr. Venayagamoorthy was an Associate Editor of the IEEE TRANSACTIONS ON NEURAL NETWORKS from 2004 to 2007 and the IEEE TRANSACTIONS ON INSTRUMENTATION AND MEASUREMENT in 2007. He is a Senior Member of the South African Institute of Electrical Engineers (SAIEE). He is also a member of the International Neural Network Society (INNS); The Institution of Engineering and Technology, U.K.; and the American Society for Engineering Education. He is currently the IEEE St. Louis Computational Intelligence Society (CIS) and IAS Chapter Chairs, the Chair of the Working Group on Intelligent Control Systems, the Secretary of the Intelligent Systems subcommittee, and the Vice-Chair of the Student Meeting Activities subcommittee of the IEEE Power Engineering Society, and the Chair of the IEEE CIS Task Force on Power System Applications. He has organized and chaired several panels, invited and regular sessions, and tutorials at international conferences and workshops. He was a recipient of the 2007 ONR Young Investigator Program Award, the 2004 NSF CAREER Award, the 2006 IEEE Power Engineering Society Walter Fee Outstanding Young Engineer Award, the 2006 IEEE St. Louis Section Outstanding Section Member Award, the 2005 IEEE Industry Applications Society (IAS) Outstanding Young Member Award, the 2005 SAIEE Young Achievers Award, the 2004 IEEE St. Louis Section Outstanding Young Engineer Award, the 2003 INNS Young Investigator Award, the 2001 IEEE CIS Walter Karplus Summer Research Award, five prize papers from the IEEE IAS and IEEE CIS, a 2006 Missouri S & T School of Engineering Teaching Excellence Award, a 2007 Missouri S & T Teaching Commendation Award, and a 2007 Missouri S & T Faculty Excellence Award. He is listed in the 2007 and 2008 editions of *Who's Who in America*, 2008 edition of *Who's Who in the World* and 2008 edition of *Who's Who in Science and Engineering*.

Sandhya Rani Jetti (S'05) received the B.Tech. degree in electrical and electronics engineering from Jawaharlal Nehru Technological University, Hyderabad, India, in 2005, and is currently pursuing the M.S. degree in electrical engineering from the Missouri University of Science and Technology, Rolla (Missouri S & T).

Currently, she is a Graduate Research Assistant in the Real-Time Power and Intelligent Systems (RTPIS) Laboratory at Missouri S & T. Her research interests are in the applications of computational intelligence techniques for power system stability and control.